Extended Energy Management Methods for Flight Performance Optimization

Anthony J. Calise*
Dynamics Research Corp., Wilmington, Mass.

This paper develops a singular perturbation approach to extend existing energy managment (*EM*) methods. A procedure is outlined for modeling altitude and flight path angle dynamics which are ignored in *EM* solutions. It is shown that nonlinear feedback solutions can be obtained, even for *EM* problem formulations which currently result in a two-point boundary-value problem. A nonlinear controller for two-dimensional, minimum time aircraft climbs is derived and numerical results for a fighter aircraft are given. The procedure outlined in this paper is general and applicable to solving a wide class of optimal control problems. It avoids the problem of picking the unknown boundary conditions at the initial and terminal times to suppress the unstable modes in the boundary layer.

Introduction

OPTIMAL control theory long has been recognized by researchers and analysts as having serious shortcomings in practical applications. The difficulty of solving nonlinear two-point boundary-value problems has prevented the widespread use of this theory as a practical analysis and design tool. In addition, real-time applications generally are limited to situations where a solution in feedback form can be found. The problems associated with applying linear-quadratic theory to systems with nonlinear dynamics are well known.

Reduced order modeling techniques have been used to overcome the mathematical difficulties associated with using optimal control theory, and to obtain nonlinear solutions in feedback form. In problems dealing with atmospheric flight performance optimization, these techniques have resulted in energy state approximation.[1,2] In some applications, the faster dynamics ignored using these approximations have a negligible effect on performance. In other cases, the energy state approximations are not sufficiently accurate or are not applicable.

Singular perturbation theory offers the unique advantage that the fast dynamics ignored in the reduced order formulation can be accounted for later through a separate "boundary-layer" analysis. The result is that the solution of a high-order problem is approximated by the solution of a series of problems of lower order.[3-5] When applied to flight performance optimization, the boundary-layer solutions can be used to extend the validity of the existing energy management (*EM*) solutions.

An outline of the paper is as follows. First, existing *EM* methods are discussed, so that the reader has a firm understanding of the approximations made and the limitations that exist in problem ormulation. A procedure then is outlined for applying singular perturbation methods to extend the *EM* methods. The extended energy management (*EEM*) solutions are inherently more accurate, and there is greater flexibility in the original problem formulation with regard to obtaining solutions in feedback form. Several examples are carried out to illustrate the solution procedure.

EM Methodology

Introducing the concept of energy state results in the following point mass equations of motion for two-dimensional flight

$$\dot{E} = (T-D)\ V/W \tag{1}$$

$$\epsilon \dot{h} = V \sin\gamma \tag{2}$$

$$\epsilon^2 \dot{\gamma} = g[\ (L/W) - \cos\gamma\ ]/V \tag{3}$$

where E is the total energy per unit weight, T is thrust, L is lift, D is drag, W is weight, g is gravity, h is altitude, and γ is flight path angle. The velocity V is regarded as a function of E and h

$$V = [2g(E-h)\ ]^{1/2} \tag{4}$$

The parameter ϵ nominally equals one.

EM methods embody the use of E as a state along with the approximations that near-level flight conditions persist over a large portion of the trajectory. Taking T and D as general nonlinear functions of h, V, and L

$$T = T(h,V) \tag{5}$$

$$D = D(h,V,L) \tag{6}$$

and assuming $\gamma = 0$ and $L = W$ in Eq. (1) results in a reduced order model

$$\dot{E} = f_E(h,E) \tag{7}$$

with h as a control variable. In the context of an optimal control problem, the energy-state approximations imply that the optimal control h varies slowly over most of the trajectory, but it may contain discontinuities and rapid variations confined to narrow regions. Zoom climbs and dives provide rapid variations in h by the interchange of kinetic and potential energy whereas E remains relatively constant. Hence, on the time scale in which energy changes are made, it is consistent to use altitude as a control variable. The concepts are better defined in mathematical terms in the context of singular perturbation theory.

Optimal Feedback Control Solutions

With the reduced order model of Eq. (7), it is possible to find optimal control solutions for several important problem formulations.[2] For example, the minimum time and fixed throttle minimum fuel paths for gaining energy are given by

$$h^* = \arg\max_h \{f_E\} \qquad \text{(minimum time)} \tag{8}$$

Presented as Paper 75-30 at the AIAA 13th Aerospace Sciences Meeting, Pasadena, Calif.; Jan. 20-22, 1975; submitted Jan. 31, 1975; revision received Nov. 24, 1976.

Index category: Aircraft Performance.

*Program Manager, Systems Analysis Department.

and

$$h^* = \arg\max_h \{f_E/(-\dot{m})\} \quad \text{minimum fuel} \tag{9}$$

for a given E, where $\dot{m}$ is the rate of change of mass at a fixed throttle setting. Equations (8) and (9) are particularly useful in that they result in unique paths in the hV plane, independent of the boundary conditions on E. Hence, a feedback solution is obtained since h^* is only a function of the current energy state. Typical paths resulting from (8) and (9) are shown in Fig. 1.

Not all formulations result in a feedback path. For example, the problem of maximizing range for a fixed throttle setting and fixed amount of fuel results in the following two-point boundary-value problem (*TPBVP*):

$$(\mathrm{d}/\mathrm{d}m)E = f_E(h,E)/(-\dot{m}), \quad E(m_0) = E_0 \tag{10}$$

$$(\mathrm{d}/\mathrm{d}m)\lambda_E = -\partial H/\partial E, \quad \lambda_E(m_f) = 0 \tag{11}$$

$$h^* = \arg\max_h \{H\}\Big|_E \tag{12}$$

where

$$H = V/(-\dot{m}) + \lambda_E f_E(h,V)/(-\dot{m}) \tag{13}$$

A single feedback path does not result from (12) since H depends on λ_E, which is a function of E_0 and m_f. The application of *EM* methods to three-dimensional problems also generally results in a *TPBVP*.[6-8]

Limitations of *EM* Approach

EM solutions do not account for the time and fuel spent in h and γ transitions. Hence, performance studies generally are limited to ranges of boundary conditions resulting in long flight times. Figure 2 illustrates this by showing a typical comparison of the minimum time *EM* solution with optimal solutions where h and γ dynamics are modeled. The *EM* solution consists of the locus of solutions to Eq. (8) across all energy levels. The time to change energy levels is given by

$$T_{\Delta E} = \int_{E_0}^{E_f} \frac{\mathrm{d}E}{\dot{E}^*} \tag{14}$$

where $\dot{E}^*$ is the energy rate on the solution path. Note that instantaneous transitions at the initial and terminal times are implied to satisfy boundary conditions on h, V, and γ. Also, there may be an intermediate region (line ab) requiring large flight path angle rates in order to follow the *EM* solution path. The performance measure in Eq. (14) is valid whenever the net change in energy is large or the boundary conditions are close to the *EM* path. The flight time and optimal path for short-term energy gains or for boundary conditions far removed from the *EM* path are not represented accurately. For these cases the optimal solution paths are dominated by transitional arcs, with a small amount of the total time spent near the *EM* solution path.

A second and perhaps more important limitation of *EM* methods is that they do not always lead to a solution in the form of a feedback path. Solutions which require iteration are cumbersome to use in performance studies and require on-board storage of parameter tables in real-time applications. In the next section a procedure is outlined for extending *EM* methods to account for the fast h and γ dynamics. It also is shown that feedback solutions can be obtained for *EM* problem formulations which currently result in a *TPBVP*. The examples given are for two-dimensional problems; however, the approach is general and can be used to obtain feedback solutions to problems in three dimensions.[5] Previous simulation studies of combat aircraft[9] and a ramjet propelled cruise missile[10] have demonstrated the accuracy of the approach.

Singular Perturbations for Extending *EM* Methods

Numerous papers discuss the use of singular perturbation methods in the solution of variational problems.[3,5,11-13] In general the techniques are based on boundary-layer solution methods of Vasil'eva and others[14,15] and can be viewed simply as a series expansion approach to solving differential equations.

The greatest difficulty encountered in applying singular perturbation methods lies in finding matching "inner expansion" (boundary-layer) solutions needed to correct for discrepancies in the so-called "fast variables." These discrepancies generally occur at the initial and terminal times. In the context of Fig. 2, the inner expansions can be used to model the h and γ transitions to and from the *EM* solution path. These expansions also are required to appropriately model discontinuities in h^* occurring along the *EM* solution path. If the initial state is given, the adjoint variables for the inner expansion system are free at the initial time and must be picked to suppress unstable modes, so that h and γ asymptotically approach h^* and γ^* on the *EM* path. For the general nonlinear case, finding the matched asymptotic solutions is a difficult problem.

In the following section an approach is outlined which avoids the problem of picking the unknown adjoint values in the inner expansion system. This is done on the basis of

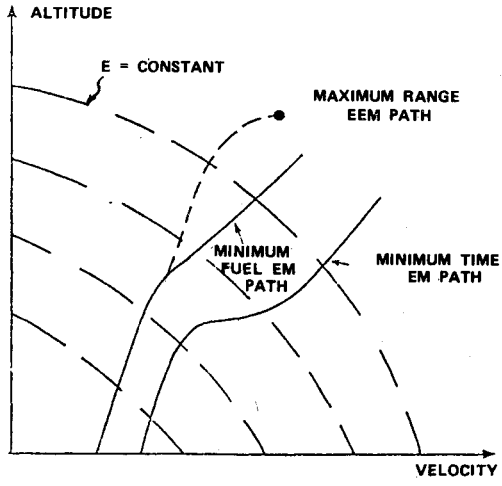

Fig. 1 Feedback solution paths resulting from energy state approximations.

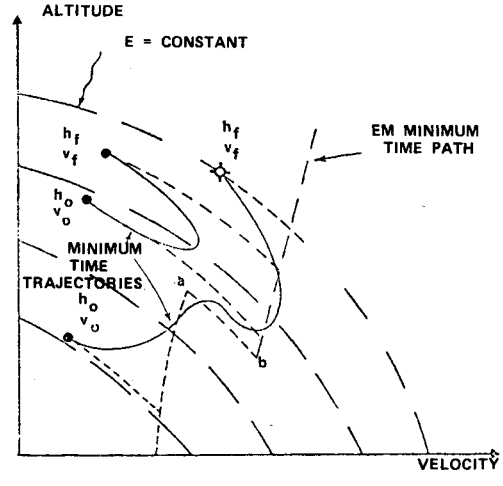

Fig. 2 Comparison of a typical EM minimum time solution path with minimum time trajectories for two sets of boundary conditions.

multiple time scale separation of the state equations,[3] and enforcing the condition that the Hamiltonian be continuous across the inner expansion for each time scale. The effects of state and control constraints are ignored to simplify the outline.

Outline of the Approach

Consider the system of equations

$$\dot{x}=f(x,y,u,t) \tag{15}$$

$$\epsilon^i \dot{y}_i = g_i(x,y,u,t),\ i=1...m \tag{16}$$

where x, y, and u are n, m, and p dimensional vectors, respectively. The parameter ϵ is introduced as a time-scaling parameter so that the individual elements of y are ordered on separate time scales in accordance with the relative speeds with which these variables can change their magnitudes.

It is desired to minimize

$$J=\phi(x,y)+\int_0^{t_f} L(x,y,u,t)\,\mathrm{d}t \tag{17}$$

The associated adjoint equations are

$$\dot{\lambda}_x = -\partial H/\partial x \tag{18}$$

$$\epsilon^i \dot{\lambda}_{y_i} = -\partial H/\partial y_i, \quad i=1...m \tag{19}$$

where

$$H=\lambda_x f+\lambda_y g+L \tag{20}$$

It is possible to write an "outer expansion" (freestream) solution of the form

$$\bullet\ (t,\epsilon)=\bullet\ (t,0)+(\partial\bullet\ /\partial\epsilon)\epsilon+... \tag{21}$$

in the state, adjoint, and control variables. However, the expansion is not uniformly valid in the interval $0\le t\le t_f$, since $y(t,\epsilon)$ and $\lambda_y(t,\epsilon)$ will not satisfy their respective boundary conditions. This leads to the occurrence of boundary layers, which can be investigated using the time stretching transformations

$$\tau_i=t/\epsilon^i, \quad \sigma_i=(t_f-t)/\epsilon^i \tag{22}$$

at the initial and terminal times, respectively.

Zero-Order Outer Expansion Solution

Taking the limit $\epsilon\to 0$, Eqs. (15) and (16) become

$$\dot{x}^0=f(x^0,y^0,u^0,t) \tag{23}$$

$$0=g_i(x^0,y^0,u^0,t) \tag{24}$$

where the superscript 0 denotes the zero-order term in the outer expansion (21). The fast variables are approximated as being infinitely fast, thus achieving their equilibrium condition (24) in zero time. The necessary conditions for optimality become

$$\dot{x}^0=f(x^0,y^0,u^0,t), \quad x^0(0)=x_0 \tag{25}$$

$$0=g(x^0,y^0,u^0,t) \tag{26}$$

$$\dot{\lambda}_x^0=-\frac{\partial H}{\partial x^0}, \quad \lambda_x^0(t_f)=\frac{\partial\phi}{\partial x^0}+\nu^T\frac{\partial\psi}{\partial x^0} \tag{27}$$

$$\partial H^0/\partial u=0, \quad \partial H^0/\partial y_i=0 \tag{28}$$

$$H^0=\lambda_x^0 f+\lambda_y^0 g+L(x^0,y^0,u^0,t) \tag{29}$$

and ψ represents the terminal constraints. Note that as a result of letting $\epsilon\to 0$ in Eq. (19), the original fast variables now appear as control variables. Also, the adjoint vector λ_y^0 in Eq.(29) now is used to enforce the constraints in Eq.(26), consequently the vectors y^0 and λ_y^0 no longer satisfy their respective boundary conditions.

All of the existing *EM* modeling can be viewed in the context of a zero-order outer expansion solution. For example, letting $\epsilon\to 0$ in Eqs. (2) and (3) results in the standard energy state approximation. The fact that h appears as a control variable now is understood in the context of the preceding paragraph.

Example 1

Consider the minimum time and minimum fuel to gain energy problems. Equations (28) and (29) become†

$$H^0=\lambda_E^0 f_E+1=0 \quad \text{(minimu time)},$$

$$\partial H^0/\partial h=0, \quad \gamma=0, \quad L=W \tag{30}$$

and

$$H^0=\lambda_E^0 f_E-\dot{m}=0 \quad \text{(minimum fuel)},$$

$$\partial H^0/\partial h=0, \quad \gamma=0, \quad L=W \tag{31}$$

where f_E is defined previously by Eq. (7). Equations (30) and (31) each represent two equations in two unknowns (h^0 and λ_E^0). The solution yields the results in Eqs. (8) and (9), along with the adjoint values

$$\lambda_E^0=-1/f_E(h^*,E) \qquad \text{minimum time} \tag{32}$$

$$\lambda_E^0=\dot{m}/f_E(h^*,E) \qquad \text{minimum fuel} \tag{33}$$

Zero-Order Boundary-Layer Solution

In this section the $i=1$ zero-order boundary-layer solution is derived for the initial time. The derivation of the remaining zero-order boundary-layer solutions follows by induction. In general, the state variables $y_{i+1}...y_m$ appear as control variables in the ith layer. The dynamics for attaining the optimal state value $y_{i+1}(\tau_{i+1})$ are modeled in the $i+1$ layer using the transformation $\tau_{i+1}=t/\epsilon^{i+1}$.

Using $\tau_1=t/\epsilon$ results in the $i=1$ initial boundary-layer system

$$(\mathrm{d}/\mathrm{d}\tau_1)x=\epsilon f[x,y,u,\epsilon_1\tau_1] \tag{34}$$

$$(\mathrm{d}/\mathrm{d}\tau_1)y_1=g_1[x,y,u,\epsilon_1\tau_1] \tag{35}$$

$$\epsilon^{i-1}(\mathrm{d}/\mathrm{d}\tau_1)y_i=g_i[x,y,u,\epsilon_1\tau_1],\ i=2...m \tag{36}$$

and the related adjoint equations

$$(\mathrm{d}/\mathrm{d}\tau_1)\lambda_x=-\epsilon(\partial/\partial x)H_1 \tag{37}$$

$$(\mathrm{d}/\mathrm{d}\tau_1)\lambda_{y_1}=-(\partial/\partial y_1)H_1 \tag{38}$$

$$\epsilon^{i-1}(\mathrm{d}/\mathrm{d}\tau_1)\lambda_{y_i}=-(\partial/\partial y_i)H_1, \quad i=2...m \tag{39}$$

where

$$H_1=\lambda_x f+\lambda_y g+L(x,y,u,\epsilon_1\tau_1) \tag{40}$$

Again, it is possible to write an inner expansion solution of the form

$$\bullet(\tau_1,\epsilon)=\bullet(\tau_1,0)+(\partial\bullet/\partial\epsilon)\epsilon+... \tag{41}$$

†The terms corresponding to $\lambda_y^0 g$ in Eq. (19) are avoided by substituting the solutions $\gamma=0$ and $L=W$ as in Eq. (7). The alternative would involve evaluating λ_y^0 using $\partial H^0/\partial\gamma=\partial H^0/\partial L=0$.

in the state, adjoint, and control variables. Equation (35) now will be used to "match" the initial conditon on y_1 to the optimal value y^0 resulting from the zero-order outer expansion solution. The zero-order boundary layer necessary conditions result from taking the limit $\epsilon \to 0$ in Eqs. (34-39).

$$(d/d\tau_1)x^0(\tau_1) = 0, \qquad x^0(\tau_1)\Big|_{\tau_1=0} = x_0 \tag{42}$$

$$(d/d\tau_1)y_1^0(\tau_1) = g_1[x_0, y^0(\tau_1), u^0(\tau_1), 0], \quad y_1^0(\tau_1)\Big|_{\tau_1=0} = y_0 \tag{43}$$

$$0 = g_i[x_0, y^0(\tau_1), u^0(\tau_1), 0], \quad i = 2...m \tag{44}$$

$$(\partial/\partial u^0)H_1^0 = 0, \quad (\partial/\partial y_i^0)H_1^0 = 0, \quad i = 2...m \tag{45}$$

where

$$H_1^0 = \lambda_x^0(0)f[x_0, y^0(\tau_1), u^0(\tau_1), 0] + \lambda_y^0(\tau_1)g[x_0, y^0(\tau_1), u^0(\tau_1), 0] + L[x_0, y^0(\tau_1), u^0(\tau_1), 0] = H^0 \tag{46}$$

Note that a feedback solution always will result from the application of Eqs. (44-46). The controls, states, and adjoints u^0, y_i^0 and $\lambda_{y_i}^0$ $(i = 2...m)$ can be evaluated using Eqs. (44) and (45). The remaining unknown adjoint $\lambda_{y_1}^0(\tau_1)$ is evaluated by enforcing continuity of the Hamiltonian in Eq. (46), where H^0 is the zero-order Hamiltonian value known from the zero-order outer expansion solution. This avoids the problem of having to pick $\lambda_{y_1}^0(\tau_1)|_{\tau_1=0}$ to suppress unstable modes. The following example will illustrate that the boundary-layer solutions provide asymptotically stable transitional arcs in the h and γ variables of Example 1. These arcs can be used to match the boundary conditions to the *EM* solution paths resulting from the zero-order outer expansion solution.

Example 2

The $i = 1$ zero-order boundary-layer equations for the minimum time problem of Example 1 are

$$E(\tau_1) = E_0 \tag{47}$$

$$(d/d\tau_1)h = V\sin\gamma \tag{48}$$

$$L = W\cos\gamma \tag{49}$$

$$H_1 = \lambda_E(0)(T-D)V/W + \lambda_h V\sin\gamma + 1 = 0 \tag{50}$$

$$(\partial H_1/\partial\gamma) = 0 \tag{51}$$

The superscript notation has been dropped for convenience in writing the equations. Employing a conventional representation for drag

$$D = qsC_{D_0} + KL^2/qS \tag{52}$$

and substituting $W^2\cos^2\gamma$ for L^2, the variation in Eq. (51) results in

$$\lambda_h(\tau_1) = -2\lambda_E(0)KW\sin\gamma(\tau_1)/q(\tau_1)S \tag{53}$$

Substituting Eq. (53) into Eq.(50) to eliminate λ_h gives the following expression for $\sin\gamma(\tau_1)$ as a function of states and known parameters

$$\sin\gamma^*(\tau_1) = \pm\sqrt{H^0(h)q(\tau_1)S/\lambda_E(0)KWV(\tau_1)} \tag{54}$$

Where $H^0(h)$ is the reduced order Hamiltonian given in Eq. (30) evaluated for $L = W$ at the current values of h and V. Since the minimum of H^0 is at $h = h^*(E_0)$ and $H^0(h^*) = 0$, it follows that $H^0(h) > 0$ for $h \neq h^*$. Note from Eq. (32) that $\lambda_E(0)$ is negative so that the argument under the radical in Eq. (54) is negative. Since there is no real solution to Eq. (54), $\gamma(\tau_1)$ must lie on the bound $(\pm\gamma_{\max})$ everywhere except at $h = h^*$ where $\gamma(\tau_1) = 0$. This implies two jumps in $\gamma(\tau_1)$, one at $\tau_1 = 0$ from the initial condition to $\pm\pi/2$ (depending on whether the initial altitude is above or below h^*) and one at $\tau_1 = \tau_1^*$ (when $h(\tau_1^*) = h^*$) from $\pm\pi/2$ to 0. Hence two boundary-layer corrections are needed to model these rapid transitions in flight path angle. Note that when $\gamma(\tau_1)$ is on the bound, $\lambda_h(\tau_1)$ is obtained from Eq. (50) as

$$\lambda_h(\tau_1) = -\frac{1 + \lambda_E(0)[T - q(\tau_1)SC_{D_0}]V(\tau_1)/W}{V(\tau_1)\sin\gamma^*(\tau_1)} \tag{55}$$

$$\gamma^*(\tau_1) = \pm\gamma_{\max} \tag{56}$$

Following the same procedure, the $i = 2$ zero-order boundary-layer equations around $\tau_1 = 0$ are

$$E(\tau_2) = E_0, \qquad h(\tau_2) = h_0 \tag{57}$$

$$(d/d\tau_2)\gamma = g[L/W - \cos\gamma]/V \tag{58}$$

$$H_2 = \lambda_E(0)(T-D)V/W + \lambda_h(0)V\sin\gamma + \lambda_\gamma g[L/W - \cos\gamma]/V + 1 = 0 \tag{59}$$

$$\partial H_2/\partial L = 0 \tag{60}$$

Equations (59) and (60) now are used to solve for $\lambda_\gamma(\tau_2)$ and $L(\tau_2)$. To simplify this step, $L(\tau_2)$ is defined as the sum of two components

$$L(\tau_2) = L_0(\tau_2) + \delta L(\tau_2) \tag{61}$$

where

$$L_0 = W\cos\gamma(\tau_2) \tag{62}$$

and the variation in Eq. (60) is taken with respect to δL. This results in the following expression

$$-2K\lambda_E(0)(L_0 + \delta L)V/qSW + \lambda_\gamma g/WV = 0 \tag{63}$$

Substitution of Eq. (63) into Eq. (59) to eliminate λ_γ provides the final expression for the zero-order lift solution as a function of states and known parameters evaluated in the zero-order outer expansion and $i = 1$ inner expansion solutions

$$\delta L = \pm\sqrt{H_1[\lambda_E(0), \lambda_h, E(0), h, L_0, \gamma]qSW/\lambda_E(0)KV} \tag{64}$$

where $H_1(\cdot)$ is defined in (50).

Note that all of the terms under the radical except γ are constants in the τ_2 time scale. Assuming that $h_0 > h^*(E_0)$, then $\gamma^*(\tau_1) = -\pi/2$ and the minus sign in Eq. (64) applies in the initial $i = 2$ boundary layer. The values of λ_h, h, V, and γ used to evaluate the terms under the radical are the current state values. In the $i = 2$ boundary layer around $\tau_1 = \tau_1^*$, the time scale transformation is

$$\sigma_2 = (\tau_1^* - t)/\epsilon_2 \tag{65}$$

For $h_0 > h^*(E_0)$ the plus sign in Eq. (64) is used and the equations of motion are in effect solved backwards in time from $h = h^*(E_0)$, $V = V^*(E_0)$, and $\gamma = 0$ obtained using Eqs. (8) and (4).

Asymptotic stability in the boundary-layer solution is required for the successful application of the control solution

in Eq. (64). That is,

$$\lim_{\tau_2 \to \infty} \gamma(\tau_2) = \gamma^*, \qquad \lim_{\sigma_2 \to \infty} \gamma(\sigma_2) = \gamma^* \tag{66}$$

From Eq. (58) this will occur if $\delta L \to 0$ as $\gamma(\tau_2) \to \gamma^*$, which is guaranteed in Eq. (64) since $H_1(\cdot, \gamma^*) = 0$ from Eq. (50). It is also desirable that $\delta L = 0$ at $\sigma_2{}^* = 0$ which will provide $L = W$ at h^*, V^*, $\gamma = 0$. From Eqs. (30) and (50) we have that

$$H_1(h^*, W, 0) = H^0(h^*) = 0 \tag{67}$$

The control solution in Eq. (64) can be used to generate constant energy transition arcs that match the boundary conditions on h and V to the values h^*, V^* on the *EM* minimum time path corresponding to the initial and final energy levels. Both h and E are constant in the $i = 2$ boundary layer; however, since $\delta L(\tau_2)$ is expressed as a function of h, it is possible to integrate h and γ and update the control solution using the current values of both h and γ as new initial conditions. This can be done in both the forward τ_2 and backward σ_2 time integrations. The sequence of computations is summarized in Fig. 3.

Numerical results on this example for the case of a fighter aircraft are given later in this paper, hence further discussion on the preceding analysis is reserved for that section.

Example 3

This example is included to illustrate the *EEM* procedure for obtaining closed-loop solutions to problem formulations that result in a *TPBVP* using *EM* methods. Consider the maximum range at fixed throttle problem whose *EM* solution is given in Eqs. (10-13). Separating position and energy dynamics, the problem is formulated as

$$(\mathrm{d}/\mathrm{d}m)x = V/(-\dot{m})$$

$$\epsilon^1 (\mathrm{d}/\mathrm{d}m)E = (T - D)V/(-W\dot{m})$$

$$\epsilon^2 (\mathrm{d}/\mathrm{d}m)h = V \sin\gamma/(-\dot{m})$$

$$\epsilon^3 (\mathrm{d}/\mathrm{d}m)\gamma = g[L/W - \cos\gamma]/(-V\dot{m})$$

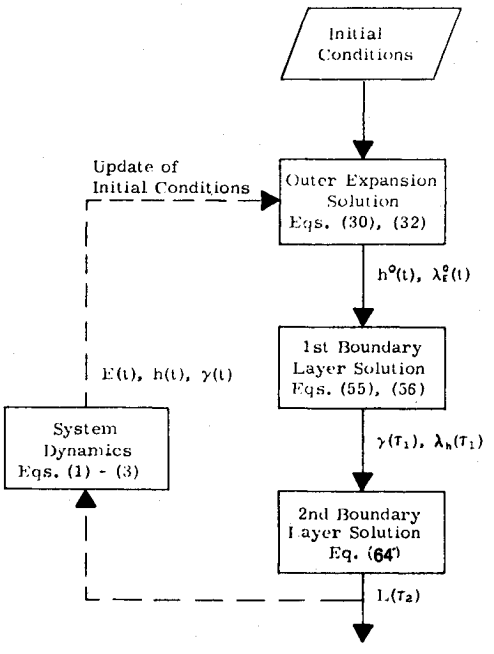

Fig. 3 Sequence of EEM computations for minimum time to climb trajectories.

with $x(m_f)$ as the performance index.

The zero-order outer solution is

$$L = W, \quad \gamma = 0, \quad T = D, \quad H^0 = \lambda_x V/(-\dot{m})$$

$$\partial H^0/\partial h = 0, \quad \partial H^0/\partial E = 0$$

Thus,

$$h^*, E^* = \arg\max_{h,E} \{V/(-\dot{m})\}\Big|_{T=D}$$

is the optimum cruise condition. Since $\lambda_x(t) = 1$, this also leads to the conclusion that $H^0 = V^*/(-\dot{m}^*)$ where V^* and $\dot{m}^*$ are the velocity and mass flow rate at the cruise condition. The zero-order, $i = 1$ boundary layer is used to model the energy gaining portion of the trajectory and the necessary conditions are the same as those in Eqs. (10-13), along with the continuity condition that $H = H^0$ in (13). This is used to evaluate the unknown adjoint λ_E and a feedback *EEM* path to the optimal cruise condition results, as illustrated in Fig. 1. Terminal constraints on h and E can be matched through the addition of appropriate zero-order terminal boundary-layer solutions.

First-Order Solution

In general the first-order necessary conditions are obtained by expanding the outer and boundary-layer necessary conditions to first order in ϵ. This is accomplished most easily by taking the variation with respect to ϵ on both sides of the equations and letting $\epsilon \to 0$. The boundary conditions to first order are derived by asymptotically matching the outer expansion to the first boundary-layer expansion. The procedure parallels that given in Ref. 18 where boundary conditions are derived by matching the outer expansion solution for small t to the boundary-layer solution for large τ. For the case here of $(n-1)$ boundary layers there are an additional $(n-1)$ adjacent boundary layers to be matched. In matching the ith boundary layer to the $i+1$ boundary layer, the solutions are matched for small τ_i and large τ_{i+1}. A similar approach is followed in the terminal boundary layers. The matching would start with the innermost boundary layers and proceed outward to the outer solution. This provides initial conditions for the first-order terms. The necessary conditions then are solved inward to the innermost boundary layer as outlined for the zero-order solution. This provides the first-order correction to the control solutions.

Although the procedure is straightforward it is cumbersome to express in mathematical terms. An example first-order expansion of the altitude and flight angle dynamics is provided in the next section.

Numerical Results

This problem is particularly well suited for numerical illustration. First, it represents a fairly complete, nonlinear aerodynamic problem. Second, its solution has been treated extensively in the literature using a spectrum of approaches including steepest ascent,[16] energy management,[1,2] and singular perturbation methods.[17-19] In Ref. 17 the parameter ϵ represents the inverse of $(L/D)_{\max}$. The zero-order outer solution is made up of singular arc energy climbs and transition arcs ($\gamma = \pm\pi/2$) with discontinuities at the junctures. The boundary-layer analysis exposes the rapid γ dynamics in the vicinity of the junctures. In Refs. 18 and 19 E is taken as the slow state with h and γ treated as fast variables that vary on the same time scale. Hence, it is necessary to solve a two-state *TPBVP* in the boundary layer. The solution is carried to first order for "Airplane 2" of Ref. 2 and is shown to compare accurately with gradient solutions obtained for the original three-state model. It also is shown in Ref. 18 that the dynamics in h and γ and their adjoints are highly coupled, which is a third reason for selecting this problem to illustrate the *EEM* analysis procedure. The closed-form solution ob-

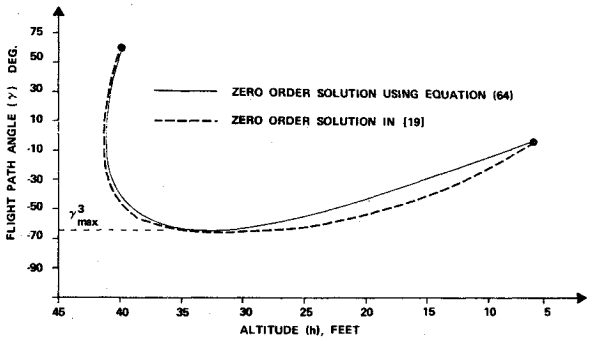

Fig. 4 Comparison of the zero-order separation of h and γ with the two-state zero-order solution for $\gamma(0) = -2.0$.

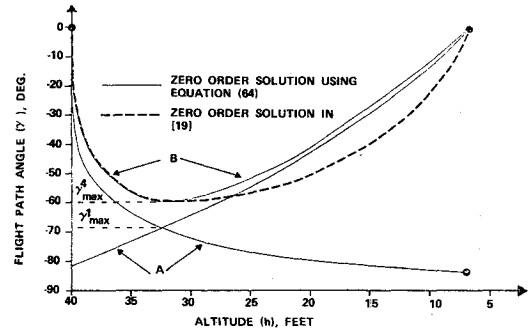

Fig. 5 Comparison of the zero-order separation of h and γ with the two-state zero-order solution for $\gamma(0) = 60$.

tained here relies on the separability of the h and γ dynamics. It is shown that accurate results are achievable through a modification of the matching procedure, thus justifying the use of separate time scales for h and γ.

The analysis in this section is confined to examining the $i=1$ and $i=2$ boundary-layer solutions in h and γ to zero and first order. Numerical comparisons are made to the zero-order solutions for h and γ in Ref. 19, which can be viewed as exact optimal solutions for the case of constant energy. Hence, the term "optimal" is used when referring to these solutions. The limited comparison here suffices to illustrate the concepts presented earlier in this paper and to demonstrate the separability of the h and γ dynamics.‡

Zero-Order Solution

The construction of the zero-order solution using Eq. (64) as the nonlinear controller has been discussed at the end of Example 2. Numerical results for the same aircraft used in Ref. 19 are given in Fig. 4 for $h(0) = 4000$ ft, $V(0) = 484$ fps and $\gamma(0) = -2°$. The energy level for $h(0)$, $V(0)$ is $E(0) = 43{,}637.5$ ft, and the corresponding optimum altitude for maximum $\dot{E}$ computed using (8) is $h^* = 7500$ ft. The E state was held constant in the simulation for comparison to the optimal solutions in Ref. 19. The curves labeled A correspond to a forward and backward time integration of the h and γ dynamics for λ_h evaluated using Eq. (55) and $\gamma_{max} = \pi/2$. Note that the boundary layers intersect before reaching their steady-state values. This is a consequence of the highly coupled h and γ dynamics. The matching condition requires that there be a region of overlap in which both the initial and terminal boundary layers are in steady state ($d\gamma/dh = 0$). The procedure used here to attain this region is to reduce γ_{max}. This corresponds to the state constraint matching technique in Ref. 20. If in the optimal solution to the three-state problem $\gamma(t) > -\gamma_{max}$, then it is convenient to think of $\gamma_{max} < \pi/2$ as an artificial constraint that does not alter the original problem statement. A logical choice for γ_{max} is the value of γ corresponding to the intersection of the A curves. This produces new values for λ_h in Eq. (55) and δL in (64), and results in a new set of curves for $\gamma = f(h)$ that intersect at a higher value for γ. This procedure was iterated until a sufficiently small value of $d\gamma/dh$ was observed at the point of intersection. The curves labeled B in Fig. 4 correspond to the numerical solution after four iterations. Also shown is the numerical result for the two-state solution given in Ref. 19. Figure 5 presents the same comparison for $\gamma(0) = 60°$. Convergence in this case was obtained after three iterations. In both cases the minimum values of γ agree to within a degree for both solution methods.

First-Order Solution

For the *EEM* analysis procedure to be valid it is necessary that the $i=1$ and $i=2$ boundary-layer control expansion be convergent to the zero-order solution of the two-state problem. The following analysis expands the control solution in (64) to first order.

Assuming that the states h, E, V, and γ are measurable functions, it is only necessary to expand λ_h and λ_E to first order to express the control solution to first order. Furthermore, since we wish to obtain a comparison to the zero order solution in Ref. 19, the first-order correction to λ_E is ignored. Hence, the control solution in Eq. (64) can be approximated to first order as

$$\delta L = \pm\sqrt{H_1(\lambda_E(0), \lambda^0_{h_2} + \lambda^1_{h_2}, E(0), h, L_0, \gamma) qSW/\lambda_E(0) KV} \tag{68}$$

‡In order to compare the *EEM* solution to the first-order results in Ref. 19, the outer solution must be expanded to first order to account for energy changes during the h and γ transitions.

Table 1 Comparison of h, γ, and L/W histories for $\gamma(0) = -2.0$ deg

Time	Altitude			Flight-path angle			Load factor		
	Zero-order *EEM*	First-order *EEM*	Two state model	Zero-order *EEM*	First-order *EEM*	Two state model	Zero-order *EEM*	First-order *EEM*	Two state model
0	40000	40000	40000	−2.0	−2.0	−2.0	−.896	−.900	−.901
2	39849	39848	39848	−15.5	−15.6	−15.6	−.706	−.743	−.731
4	39842	39476	39476	−26.8	−27.3	−27.2	−.550	−.597	−.581
6	38923	38907	38909	−36.0	−36.7	−36.6	−.418	−.462	−.445
8	38192	38162	38166	−43.3	−44.1	−44.0	−.300	−.332	−.381
10	37304	37258	37265	−48.9	−49.8	−49.6	−.184	−.204	−.255
12	36272	36209	36219	−53.1	−53.9	−53.8	−.070	−.075	−.066
14	35105	35026	35039	−56.1	−56.9	−56.7	−.048	.059	.066
16	33814	33718	33735	−58.2	−58.7	−58.6	.172	.206	.206
18	32406	32296	32315	−59.4	−59.7	−59.6	.303	.357	.357

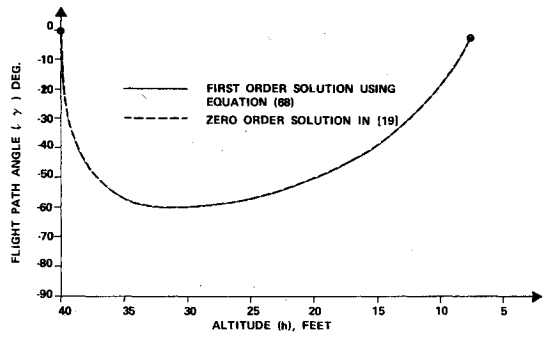

Fig. 6 Comparison of the first-order separation of h and γ with the two-state zero-order solution for $\gamma(0) = -2.0$.

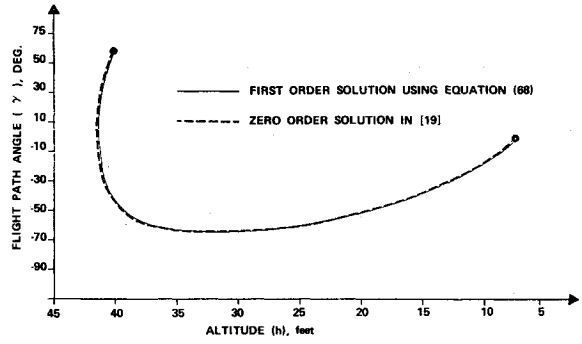

Fig. 7 Comparison of the first-order separation of h and γ with the two-state zero-order solution for $\gamma(0) = 60$.

The subscript 2 denotes a second boundary-layer expansion term and the superscript denotes the order of the expansion term. For example

$$\lambda_{h_2}^{I} \equiv (\partial/\partial\epsilon)\lambda_h(\epsilon, \tau_2)\,|_{\epsilon=0}$$

If the control is updated after each integration step and each new state is treated as an initial condition, then we require the initial conditions for $\lambda_{h_2}^{0}$ and $\lambda_{h_2}^{I}$ in Eq. (68). These are developed by applying the usual matching conditions of matched asymptotic expansion theory. Following the approach given in Refs. 18 and 19, the matching condition for λ_h between the $i=1$ and $i=2$ boundary layers is

$$\lambda_{h_2}^{0}(0) = \lambda_{h_1}^{0}(0) = \lambda_h(0) \quad \text{in Eq.(55)} \tag{69}$$

$$\lambda_{h_2}^{I}(0) = \lambda_{h_1}^{I}(0) + \tau_2^* \frac{\mathrm{d}}{\mathrm{d}\tau_2}\lambda_{h_2}^{I}(\tau_2^*) - \int_0^{\tau_2^*} \frac{\mathrm{d}}{\mathrm{d}\tau_2}\lambda_{h_2}^{I}(\tau_2)\mathrm{d}\tau_2 \tag{70}$$

where

$$\frac{\mathrm{d}}{\mathrm{d}\tau_2}\lambda_{h_2}^{I} = -\frac{\partial H_2}{\partial h}\,|^0 = -\lambda_E(0)\frac{\partial \dot{E}_2}{\partial h}\,|^0$$

$$+\lambda_{h_2}^{0}(0) g \sin\gamma/V - \lambda_{\gamma_2}^{0}(0) g^2 [L/W - \cos\gamma]/V^3 \tag{71}$$

and where $\lambda_{\gamma_2}^{0}$ is obtained using Eq. (63).

The time τ_2^* is picked sufficiently large so that $(\mathrm{d}/\mathrm{d}\tau_2)\lambda_{h_2}^{I}$ is in steady state. Equation (70) relates $\lambda_{h_2}^{I}(0)$ to $\lambda_{h_1}^{I}(0)$, which, in turn, is determined by expanding Eqs. (50) and (51) to first order. Again, ignoring the first-order terms in λ_E and E we have $\lambda_I^I = 0$ and

$$H_1^I(0) = \lambda_E(0)(\partial \dot{E}_1/\partial h) h_1^I(0) - \lambda_{h_1}^{0}(0)(g \sin\gamma_1^0/V) h_1^I(0)$$
$$+\lambda_{h_1}^{I}(0) V \sin\gamma_1^0 = 0 \tag{72}$$

where $\gamma_1^0 = -\gamma_{\max}$ from the matched zero-order solution. The term $h_1^I(0)$ in Eq. (72) is obtained from a similar matching condition to that in Eq. (70)

$$h_1^I(0) = h_2^I(0) + \int_0^{\tau_2^*} \frac{\mathrm{d}}{\mathrm{d}\tau_2} h_2^I(\tau_2)\mathrm{d}\tau_2 - \tau_2^* \frac{\mathrm{d}}{\mathrm{d}\tau_2} h_2^I(\tau_2^*) \tag{73}$$

where

$$(\mathrm{d}/\mathrm{d}\tau_2) h_2^I = V \sin\gamma \tag{74}$$

and $h_2^I(0) = 0$ since $h_2^0(0)$ already satisfies the boundary condition on h. This completes the equations needed to determine $\lambda_{h_2}^{0}$ and $\lambda_{h_2}^{I}$ in Eq. (68). The boundary-layer integrations in Eqs. (70) and (73) are done at each major integration step to update the value of $\lambda_{h_2}^{I}$.

Figures 6 and 7 show that a remarkably accurate result is obtained using the nonlinear control in Eq. (68). The accuracy is possibly due to the feedback nature of the solution which requires that only the adjoints (and not the states) be corrected to first order. The numerical comparisons of h, γ, and L/W for the initial γ boundary layer are given in Tables 1 and 2.§ A one-to-one comparison for the terminal boundary layer is not

§The numerical results for the two-state solution were provided by the author of Ref. 19 for this comparison.

Table 2 Comparison of h, γ, and L/W histories for $\gamma(0) = 60$ deg

Time	Altitude			Flight path angle			Load factor		
	Zero-order *EEM*	First-order *EEM*	Two state model	Zero-order *EEM*	First-order *EEM*	Two state model	Zero-order *EEM*	First-order *EEM*	Two state model
0	40000	40000	40000	60.	60.	60.	−1.690	−1.430	−1.443
2	40709	40721	40724	41.5	43.9	44.4	−1.460	−1.233	−1.204
4	41151	41201	41210	22.8	26.8	27.4	−1.098	−.999	.999
6	41337	41439	41453	4.8	9.1	9.6	−.825	−.822	−.822
8	41289	1445	41465	−11.5	−8.0	−7.6	−.628	−.676	−.670
10	41034	41236	41262	−25.3	−23.0	−22.8	−.482	−.546	−.538
12	40593	40835	40866	−36.4	−35.2	−35.1	−.370	−.430	−.421
14	39986	40260	40297	−45.0	−44.6	−44.5	−.274	−.323	−.315
16	39225	39527	39569	−51.4	−51.7	−51.6	−.185	−.220	−.214
18	38320	38649	38696	−56.2	−56.8	−56.7	−.097	−.118	−.115
20	37252	37606	37685	−59.8	−60.4	−60.4	.005	−.010	−.013
22	36080	36458	36545	−62.2	−62.8	−62.9	.090	.102	.095
24	34784	35188	35282	−63.8	−64.3	−64.4	.192	.224	213
26	33371	33801	33901	−64.7	−64.9	−65.1	.301	.360	.342

possible since the results were not available at identical time points due to the differences in the techniques used to generate the trajectories.

It should be pointed out that the numerical solutions given in Refs. 18 and 19 for the *TPBVP* associated with the two-state problem exhibit an instability near the energy climb path. This is because of the inability to pick the unknown adjoint at the initial time to exactly cancel the two unstable roots associated with the state adjoint system of dynamics. This problem is avoided when the h and γ dynamics are separated. An additional comment is in order with respect to the method of matching the h and γ dynamics in the zero-order solution. An exactly analogous situation exists with respect to optimal flight to a specified range (Example 3). For short ranges the climb and descent paths intersect before reaching the optimal cruise condition. For this case the cruise altitude should be constrained in computing the zero-order outer solution until the boundary-layer climb and descent arcs intersect at a point where dh/dx is near zero. An analogous procedure was used in Ref. 21 to derive minimum direct operating cost trajectories for airline short-haul missions.

Conclusions

A singular perturbation approach for extending *EM* methods has been outlined. The approach systematically accounts for the dynamics in all of the state variables and yields a solution in feedback form. Matching boundary-layer trajectories result whenever the system is controllable to the equilibrium conditions of the *EM* solution path. The problem of picking the unknown adjoint values in the boundary layers to guarantee stability is avoided by enforcing continuity of the Hamiltonian across the boundary layers.

References

[1]Rutowski, E.S., "Energy Approach to the General Aircraft Performance Problem," *Journal of the Aeronautical Sciences*, March 1954, pp.187-195.

[2]Bryson, A.E., Jr., Desai, M.N., and Hoffman, W.C., "Energy-State Approximation in Performance Optimization of Supersonic Aircraft," *Journal of Aircraft*, Vol. 6, Nov.-Dec. 1969, pp. 481-888.

[3]Kelley, H.J. "Flight Path Optimization with Multiple Time Scales," *Journal of Aircraft*, Vol. 8, April 1971, pp. 238-240.

[4]Kelly, H.J. and Edelbaum, T.N., "Energy Climbs, Energy Turns, and Asymptotic Expansions," *Journal of Aircraft*, Vol. 7, Jan. 1970, pp. 93-95.

[5]Calise, A.J., "Singular Perturbation Methods for Variational Problems in Aircraft Flight," *IEEE Transactions on Automatic Control*, Vol. AC-21, June 1976, pp.345-353.

[6]Hedrick, J.K. and Bryson, A.E., Jr., "Three-Dimensional, Minimum Time Turns for a Supersonic Aircraft," AIAA Paper 71-796, July 1971, Seattle, Wash.

[7]Hedrick, J.K. and Bryson, A.E., Jr. "Three-Dimensional Minimum Fuel Turns for a Supersonic Aircraft," AIAA Paper, 71-913, Aug. 1971, Hempstead, N.Y.

[8]Parsons, M.G., Bryson, A.E., Jr., Hoffman, W.C., "Long-Range Energy-State Maneuvers for Minimum Time to Specified Terminal Conditions," AIAA Paper 73-229, Jan. 1973, Washington, D.C.

[9]Calise, A.J., Aggarwal, R., and Anderson, G.M., "Aircraft Optimal Weapon Delivery Maneuvers Based on Extended Energy Management," AIAA Paper 75-1076, Aug. 1975, Boston, Mass.

[10]Glaros, L.N., Crigler, S.W., and Calise, A.J., "Power-Off Range Optimization Using Extended Energy Management Techniques," *13th Aerospace Sciences Meeting*, Paper No. 75-209, Jan. 1975, Pasadena, Calif.

[11]Kokotovic, P.V., "A Control Engineer's Introduction to Singular Perturbations," *Singular Perturbations: Order Reduction in Control System Design*, ASME, New York, 1972.

[12]Wilde, R.R. and Kokotovic, P.V., "Optimal Open- and Closed-Loop Control of Singularly Perturbed Linear Systems," *IEEE Transactions on Automatic Control*, Vol. AC-18, Dec. 1973, pp.616-626.

[13]Reddy, P.B. and Sannuti, P., "Optimal Control of a Coupled-Core Nuclear Reactor by a Singular Perturbation Method," *IEEE Transactions on Automatic Control*, Vol. AC-20, Dec. 1975, pp.766-769.

[14]Wasow, W.R., *Asymptotic Expansions for Ordinary Differential Equations*, Interscience, New York, 1965, Chap.10.

[15]Nayfeh, A., *Perturbation Methods*, Wiley, New York, 1973, Chap. 4.

[16]Bryson, A.E. and Denham, W.F., "A Steepest-Ascent Method for Solving Optimum Programming Problems," *Journal of Applied Mechanics*, June 1962.

[17]Breakwell, J.V., "Optimal Flight-Path Angle Transitions in Minimum Time Airplane Climbs," AIAA Paper 76-795, Aug. 1976, San Diego, Calif.

[18]Ardema, M.D., "Solution of the Minimum Time-To-Climb Problem by Matched Asymptotic Expansions," *AIAA Journal*, Vol. 14, July 1976, pp. 843-850.

[19]Ardema, M.D., "Singular Perturbations In-Flight Mechanics," NASA TM-X-62-380, Aug. 1974; revised Oct. 1975.

[20]Calise, A.J., "Singular Perturbation Analysis Approach for Systems with Highly Coupled Dynamics," *Fourteenth Annual Allerton Conference on Circuit and System Theory*, Sept.-Oct. 1976, University of Illinois, Urbana-Champaign.

[21]Ertzberger, H., Barman, J.F., and McLean, J.D., "Optimum Flight Profiles for Short Haul Missions," AIAA Paper 75-1124, Aug. 1975, Boston, Mass.